PHYSICAL REVIEW B **89**, 075102 (2014)

Structural and electronic properties of $Sr_2RuO_4/Sr_3Ru_2O_7$ heterostructures

Carmine Autieri,[1,2,3,*] Mario Cuoco,[1,2] and Canio Noce[1,2]
[1]*SPIN-CNR, I-84084 Fisciano (Salerno), Italy*
[2]*Dipartimento di Fisica "E. R. Caianiello," Università di Salerno, I-84084 Fisciano (Salerno), Italy*
[3]*IAS, Forschungszentrum Jülich, 52425 Jülich, Germany*

(Received 3 December 2012; revised manuscript received 13 January 2014; published 3 February 2014)

We carry out first-principles calculations for $Sr_2RuO_4/Sr_3Ru_2O_7$ superlattices. We show that such systems develop a significant structural rearrangement within the superlattice, which leads to a modification of the electronic structure close to the Fermi level. Compared with the pure Sr_2RuO_4 and $Sr_3Ru_2O_7$ phases, we find that the positions of the peaks in the density of states close to the Fermi levels get shifted and renormalized in the spectral weight. Then, by means of the maximally localized Wannier functions approach, we determine the effective tight-binding parameters for Ru bands and used them to discuss the modification of the electronic structure and the collective behavior of superlattice with respect to the bulk phases.

DOI: 10.1103/PhysRevB.89.075102 PACS number(s): 74.70.Pq, 71.20.−b, 74.78.Fk, 73.20.−r

I. INTRODUCTION

There is consolidated evidence that the interface between different electronic states and quantum orders is a source of novel physical phenomena [1]. The interest for this research area points both to the underlying fundamental physics as well as to the high impact in applications based on heterostructures with new emergent functionalities with respect to their constituents. Transition metal oxides (TMO) with perovskite structure are prototype systems to be exploited in this framework due to the large variety of correlated driven physical phenomena they exhibit, ranging from Mott insulator to unconventional superconductivity through all sorts of different spin-charge-orbital broken symmetry states [2]. Moreover, the recent achievements in the fabrication of atomically controlled TMO-based interfaces explain why they represent a unique opportunity to explore how spin, charge, and orbital reconstruction at the interface may determine novel quantum states of matter [3–9]. From a general point of view, the reduced dimensionality at the interface is certainly a driving force for setting novel quantum phases as it may enhance the electronic correlations against the kinetic energy. On the other hand, the degree of matching of the TMO forming the heterostructure, the character of the transition elements, and how they get into contact at the interface are the source of complexity and of a wide variety of physical properties.

In this context, the Ruddlesden-Popper (RP) family $Sr_{n+1}Ru_nO_{3n+1}$ of Sr-based ruthenates, with n being the number of RuO_2 layers in the unit cell, offers a distinct perspective for designing interfaces of TMOs made of homolog chemical elements. Furthermore, they exhibit a different character of the broken symmetry states and their properties range from unconventional p-type superconductivity [10] to metamagnetism [11] or proximity to a quantum critical point [12,13] along with the notable magnetic effects [14–17] as a function of n.

Two recent experimental achievements have triggered significant interest in interfaces made by ruthenate RP members. First, the presence of an eutectic point in the chemical phase diagram of the SrRuO perovskites allows one to get natural interfaces in the form of single crystalline micrometric domains between adjacent members of the series. In this respect, we mention that $Sr_2RuO_4/Sr_3Ru_2O_7$ [18,19] and $Sr_3Ru_2O_7/Sr_4Ru_3O_{10}$ [20] eutectics have been achieved. The investigation of the collective behavior of the eutectic phases indicates a relevant role of the interface physics, and their superconducting and magnetic properties turn out to differ markedly if compared to the homogeneous single crystalline ones [21–23].

The other important reason to study interfaces made of Sr-based ruthenates is that thin films of the series from $n = 1$ to $n = 5$ [24,25] have been successfully grown. While the magnetic states are usually obtained in the Sr-RP members in the shape of thin films, it is quite remarkable to underline the recent preparation [26] of superconducting thin films of Sr_2RuO_4 whose difficulty is due to the strong sensitivity of the spin-triplet pairing to disorder. Thus, the synthesis of superlattices based on different RP members is, in principle, an achievable task, increasing the research in designing superlattices or heterostructures by fully employing the different character of the broken symmetry states realized within the Sr-RP family as a function of n.

Taking into account the above-mentioned motivations, the aim of the paper is to analyze the structural and electronic properties of $Sr_2RuO_4/Sr_3Ru_2O_7$ superlattices. We use a first-principles density functional theory (DFT) to determine the fully relaxed volume and the atomic positions as well as the electronic structure of heterostructure made with $n = 1$ and $n = 2$ elements. The maximally localized Wannier functions approach is then applied to extract the effective tight-binding parameters between the $4d$ Ru orbitals in the superlattice at the interface and within the Sr_2RuO_4 and $Sr_3Ru_2O_7$ unit cells. The outcome is used to discuss the modification of the electronic structure of the superlattice, as well as its interrelation with the structural properties and the bulk phases. The focus is on two superlattice structures shown in Figs. 1(c) and 1(d) of the type $(Sr_2RuO_4)_l/(Sr_3Ru_2O_7)_m$ with $(l,m) = (3,3)$ and $(4,2)$, l and m being the number of $n = 1$ and $n = 2$ unit cells in the heterostructure, respectively. These configurations

---

[*] Present address: Department of Physics and Materials Science, Uppsala University, Box 530, SE-75121, Uppsala, Sweden.

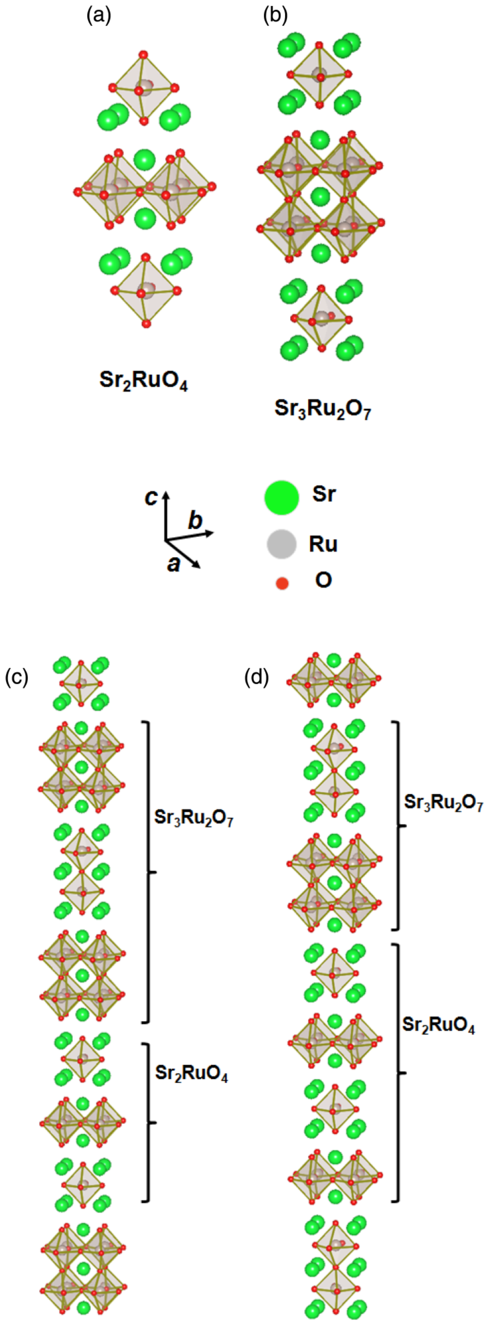

FIG. 1. (Color online) Structure of the (a) Sr_2RuO_4 and (b) $Sr_3Ru_2O_7$ bulk phases as well as of the (c) $(Sr_2RuO_4)_3/(Sr_3Ru_2O_7)_3$ and (d) $(Sr_2RuO_4)_4/(Sr_3Ru_2O_7)_2$ superlattices.

consist of at least an interface layers block that is inequivalent to the inner one within the $n = 1$ or the $n = 2$ side of the heterostructure. This allows one to extract the structural and the electronic features of the different RuO_2 layers depending on the character of the neighboring ones.

Moreover, we discuss in detail the role played by the interface. To this end, we have examined how the structural modifications of the Sr-O and Ru-O bonds affect the electronic distribution, as well as the variation of the peak positions in the density of states close to the Fermi level. We find that these peaks get shifted and renormalized in the spectral weight, compared to the bulk case, and the balance between the renormalization of the bandwidth of the d_{xy} band and the crystal field splitting results into a change of the van Hove singularities (VHS) positions in the superlattice with respect to the pure phases.

The paper is organized as follows. In the Sec. II we provide the general framework of the computational analysis. Section III is devoted to the presentation of the results concerning the structural and the electronic outcome for the Sr_2RuO_4 and $Sr_3Ru_2O_7$ bulk phases. In Sec. IV we show and discuss the outcomes of our calculations about the structural properties of $(Sr_2RuO_4)_l/(Sr_3Ru_2O_7)_m$ superlattices, while in Sec. V we give our results for the electronic properties of the superlattices. Finally, Sec. VI summarizes our results.

II. COMPUTATIONAL FRAMEWORK

Since the systems we investigate in the paper are paramagnetic, we perform spin-unpolarized first-principles density functional calculations [27] by using the plane-wave ABINIT package [28], the generalized gradient approximation (GGA) for the exchange-correlation functional [29], and ultrasoft pseudopotentials [30]. We consider a plane-wave energy cutoff of 40 Hartree and a cold smearing of 0.045 Hartree. These values are common to all the calculations. We assume for the energy differences an accuracy of 10^{-8} Hartree, compared to the values used for the plane-wave cutoff energy and Brillouin zone sampling, and we control the self-consistent procedure in a way that, when the total energy calculated in two subsequent steps is less than this value, the whole procedure is stopped. Furthermore, adopting the cold smearing, we approximate the δ function by a Gaussian multiplied by a first-order polynomial [31]. Then we first perform the calculation of the relaxed crystal structure and of the energy spectra for the Sr_2RuO_4 and $Sr_3Ru_2O_7$ bulk phases, and then we implement the same computational scheme for the superlattice. Since similar calculations have been performed already and a lot of data are available on the structural and electronic properties of the Sr_2RuO_4 and $Sr_3Ru_2O_7$ bulk phases, we can test the accuracy of this approach. In this way, we feel confident to have a controlled scheme of analysis for the homogeneous and the superlattice structures. We would note that standard functionals based on the local density approximation may tend to overestimate the volume, producing an inaccurate ratio between the c and a axes [32]. This problem is encountered for the analyzed class of ruthenate oxides, especially for the $Sr_3Ru_2O_7$ bulk phase. Thus, to get a more accurate determination of the volume and lattice constants in the study of the superlattice made of the first two RP members of the series, we employ the exchange-correlation of Wu and Cohen [29], a variant of the generalized gradient approximation by Perdew *et al.* (PBE) [33] method optimized for the relaxation of bulk systems. An $8 \times 8 \times 8$ k-point grid is used for Sr_2RuO_4, while a $8 \times 8 \times 2$ grid is used for $Sr_3Ru_2O_7$ for the full relaxation. Furthermore, the $Sr_2RuO_4/Sr_3Ru_2O_7$ hybrid structures are studied with a $4 \times 4 \times 1$ k-point grid for the full relaxation and a $8 \times 8 \times 1$ k-point grid for the determination of the density of states (DOS). To get the full relaxation of the system, we optimize the internal degrees of freedom by requiring the forces to be less than 10^{-4} Hartree/Bohr and the external pressure to be less than 0.05 GPa.

Let us consider some details about the determination of the effective tight-binding Hamiltonian in an atomic-like Wannier basis for the Sr_2RuO_4, $Sr_3Ru_2O_7$ and the superlattice configurations. There are different ways to get the Wannier functions for the relevant electronic degrees of freedom including the orthogonalized projections of specific atomic orbitals on the Bloch wave functions in a distinct energy window and downfolded muffin tin orbitals as well as maximally localized Wannier functions (MLWFs). Hereafter, to extract the character of the electronic bands at the Fermi level, we use the Slater-Koster [34] interpolation scheme based on the MLWF method [35,36]. Such an approach is applied to the determination of the real-space Hamiltonian matrix elements in the MLWF basis for the bulk Sr_2RuO_4 and $Sr_3Ru_2O_7$ phases as well as for the different superlattice configurations and to discuss the modification of the relevant parameters with respect to the structural changes. After obtaining the DFT Bloch bands, the MLWFs are constructed using the WANNIER90 code [37]. Starting from an initial projection of atomic d basis functions belonging to the t_{2g} sector and centered at the different Ru sites within the unit cell on the Bloch bands, we get a set of three t_{2g}-like MLWF for each site within the different unit cells of the analyzed systems.

We will briefly introduce the main concepts of the MLWF procedure. We start by noticing that, in general, the Bloch waves can be expressed as a Bloch sum of atomic-like basis functions or Wannier functions. Indeed, assuming to have a group of N Bloch states $|\psi_{n\mathbf{k}}\rangle$ that is isolated in energy from the other bands in the Brillouin zone (BZ), one can construct a set of N localized Wannier functions $|w_{n\mathbf{R}}\rangle$ associated with a lattice vector $\mathbf{R}$ by means of the following transformation:

$$|w_{n\mathbf{R}}\rangle = \frac{V}{(2\pi)^3}\int_{\mathrm{BZ}}\left(\sum_{m=1}^{N} U_{mn}^{(\mathbf{k})}|\psi_{n\mathbf{k}}\rangle\right)e^{-i\,\mathbf{k}\cdot\mathbf{R}}d\mathbf{k},$$

where $U^{(\mathbf{k})}$ is a unitary matrix that mixes the Bloch functions at a given $\mathbf{k}$ vector in the Brillouin zone. The choice of $U^{(\mathbf{k})}$ determines the structure of the Wannier orbitals. In Ref. [35] the authors demonstrated that a unique set of Wannier functions can be obtained by minimizing the total quadratic spread of the Wannier orbitals expressed in terms of the position operator $\mathbf{r}$ through the following relation $\Omega = \sum_{n=1}^{N}[\langle\mathbf{r}^2\rangle_n - \langle\mathbf{r}\rangle_n{}^2]$ with $\langle O\rangle_n = \langle w_{n0}|O|w_{n0}\rangle$. For the case of entangled bands, one has to introduce another unitary matrix that takes into account the extra Bloch bands in the energy window upon examination. Such a matrix is also obtained by minimizing the functional Ω [36]. Once a set of MLWFs is determined, the corresponding matrix Hamiltonian is given by a unitary transformation from the diagonal one in the Bloch basis. The resulting real-space representation of the Hamiltonian in the MLWF basis can be expressed as

$$\tilde{H} = \sum_{\mathbf{R},\mathbf{d}}\sum_{n,m} t_{nm}^{\mathbf{d}}(\tilde{c}_{n,\mathbf{R}+\mathbf{d}}^{\dagger}\tilde{c}_{m,\mathbf{R}} + \mathrm{H.c.}),$$

where $\tilde{c}_{n,\mathbf{R}}$ destroy an electron in the n orbital Wannier state $|w_{n\mathbf{R}}\rangle$. Then the real-space elements $\mathrm{t}_{nm}^{\mathbf{d}}$ can be considered effective hopping amplitudes as in a tight-binding approach between MLWF separated by a distance $\mathbf{d}$ associated with the lattice vectors.

III. BULK MATERIALS

To better analyze the results for $Sr_2RuO_4/Sr_3Ru_2O_7$ superlattices, in this section we present and discuss the electronic properties of the Sr_2RuO_4 and $Sr_3Ru_2O_7$ bulk materials. We recall that Sr_2RuO_4 has a space group $I4/mmm$, whereas, due the rotations of the octahedra, $Sr_3Ru_2O_7$ exhibits an orthorhombic symmetry with $Pban$ space group.

A. Bulk Sr_2RuO_4 phase

The low-energy physics of the Sr_2RuO_4 can be well captured by the single-particle terms of the Hamiltonian [38,39]. Indeed, apart from the tight-binding models with an analytical expression for the band dispersion near the Fermi level [40,41], it was shown that, additionally, spin-orbit effects play an important role in the low-energy regime [42–44], whereas, focusing on the many-body part, the relevance of the Hunds coupling in addition to the larger Hubbard U has been elucidated in several works [45–47]. Recently, a renewed interest for the surface electronic structure of the Sr_2RuO_4 has been yielded by the observation of an anomalous splitting of one of the band emerging from the hybridization between the d_{xz} and d_{yz} states [48–50]. Moreover, the electronic structure of Sr_2RuO_4 has been already studied by several authors by means of a density functional with the local density approximation (LDA) or GGA [39,42,51–53]. It is found that the tetravalent Ru atom has four electrons left in the $4d$ shell; the quasicubic crystal field splits the d levels into threefold degenerate t_{2g} and twofold degenerate e_g states. At the Fermi level, four electrons fill the t_{2g} bands, while the e_g bands are empty, being higher in energy. DFT calculations show that the three t_{2g} bands can be divided into a wider quasi-two-dimensional xy and two quasi-one-dimensional bands of γz character ($\gamma z = xz,yz$). While the first band does not hybridize with the others, the xz and yz mix each other by forming an electron and holelike Fermi sheets.

The electronic structure and the dispersion calculated from the t_{2g}-like MLWFs are shown in Fig. 2. The spectra and the derived Fermi surface are in agreement with those of the previous studies. As a distinct feature that will be also analyzed later for the superlattice, we note that the energy spectrum exhibits a flatness at the $M = (0,\pi)$ and $(\pi,0)$ points of the Brillouin zone leading to a van Hove singularity in the density of states above the Fermi level. The MLWFs approach provides the effective electronic parameters for the t_{2g}-atomic-like obtained Wannier functions. The resulting amplitudes are reported in the Table I along specific connecting vectors in the ab plane and along the c axis. The amplitude of the effective electronic parameters is in agreement with those deduced by means of different first-principles methods [42].

We point out that DFT calculations based on LDA [39,51,52] place the (π, 0), (0, π) saddle point of the xy band about 60 meV above the Fermi energy. By taking into account the gradient corrections, this singularity is lowered in energy to about 50 meV above the Fermi level [39], while local Coulomb correlations push the xy VHS approximately to within 10 meV, near the Fermi energy [42,53].

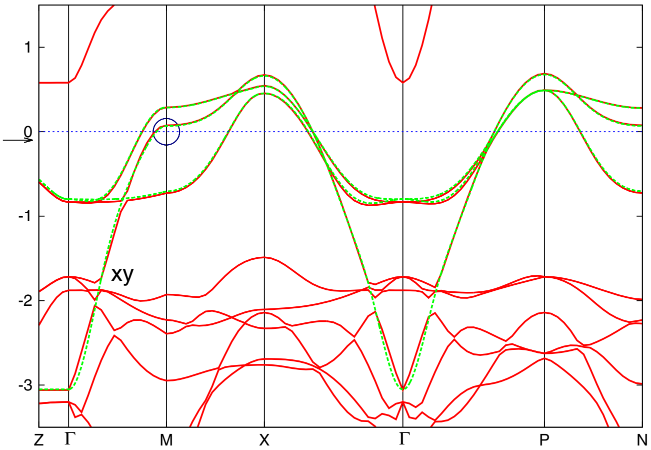

FIG. 2. (Color online) Electronic structure of Sr_2RuO_4 obtained within the density functional analysis by means of GGA (red full line) and the dispersion obtained from the t_{2g}-like MLWFs (green dotted line). The e_g levels are about 0.5 eV above the Fermi level. The Fermi level is set to zero and the energies are reported in eV. The circle indicates the position of the van Hove singularity, whose energy value is identified by the arrow.

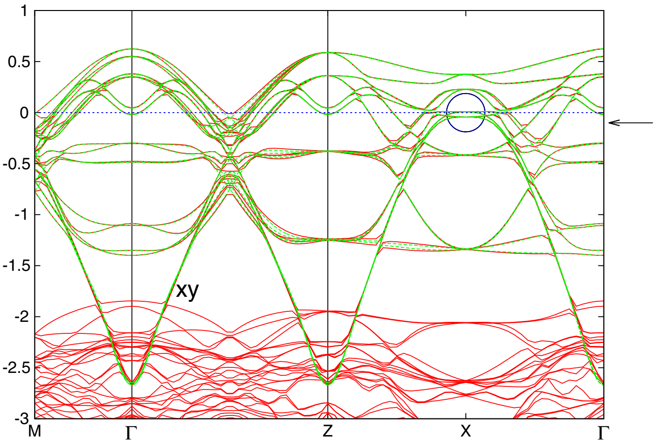

FIG. 3. (Color online) Electronic structure of $Sr_3Ru_2O_7$ obtained within the density functional analysis by means of GGA (red full line) and the dispersion obtained from the t_{2g}-like MLWFs (green dotted line). The position of the van Hove–like singularity is located in the middle of the long direction Z-Γ (*X* point). The position of the VHS, indicated by the arrow and circled in the plot, in the **k** space is the same of Sr_2RuO_4, but the crystal symmetry differs. The Fermi level is set to zero and the unit scale of the energies is eV.

Concerning the structural properties, the relaxed in-plane (out-of-plane) lattice constant *a* (*c*) turns out to be slightly larger (smaller) than the available experimental value with a resulting computed volume which is only ∼0.7% larger than the experimental one. For completeness, it is worth pointing out that the volume obtained using PBE is ∼1% larger than the experimental value [56].

1. Bulk $Sr_3Ru_2O_7$ phase

The electronic structure of $Sr_3Ru_2O_7$ has been analyzed using angle-resolved photoemission spectroscopy (ARPES) [57,58] and density functional calculations [59] with a reasonable agreement between theory and experiments. Due to the presence of two RuO_2 layers in the unit cell, there are replicas of the t_{2g} bands which are then split by the bilayer coupling and the orthorhombic distortions. Within a first approximation, the Fermi surface of the $Sr_3Ru_2O_7$ can be derived from the six t_{2g} bands (three from each RuO_2 layer) with bonding-antibonding (odd-even) splitting due to the bilayer coupling. Nevertheless, the topology of the Fermi surface is deeply modified with respect to a simple doubling of the Fermi sheets due to various factors. The bilayer splitting, the extra k_z dispersions, and the avoiding crossing between the d_{xy} and the d_{yz} bands tend to reduce the bands nesting. Furthermore, due to the orthorhombic distortions, small cylindrical lens-shaped Fermi sheets form around the *M* point (i.e., the center of the lateral face of the tetragonal Brillouin zone) and two small cylindrical sheets with almost no k_z dispersion around the Γ point.

We have performed a detailed analysis of the electronic structure of the bilayer $Sr_3Ru_2O_7$ within the GGA scheme described in the Sec. II by focusing on the case of the fully distorted orthorhombic configuration [60]. The obtained band structure, reported in Fig. 3, as well as the derived Fermi surface agree somewhat with the ARPES and the previous density functional results mentioned above. Due to the various physical factors that enter into the electronic structure and the difficulty of tracing and correlating them when a superlattice configurations is considered, we have determined the effective tight-binding parameters in the MLWFs basis.

In a tetragonal environment the MLWFs mainly correspond with the t_{2g} atomic-like states, and this is the case for the Sr_2RuO_4. The MLWFs for the $Sr_3Ru_2O_7$ differ because the

TABLE I. Hopping integrals along the direction $[lmn]$ and on-site energy in eV associated to the three orbitals of the t_{2g} sector of the bulk Sr_2RuO_4 at experimental atomic positions [54]. The connecting vector is expressed in terms of the integer set $[l\ m\ n]$ and the lattice constants a and c as $\mathbf{d} = l\,a\,\mathbf{x} + m\,a\,\mathbf{y} + n\,c\,\mathbf{z}$ [28,37,55].

Orbital index	Amplitude							
$[l\ m\ n]$	[000]	[100]	[010]	[110]	[200]	[020]	$[\frac{1}{2}\,\frac{1}{2}\,\frac{1}{2}]$	[001]
xy-*xy*	−0.4750	−0.3867	−0.3867	−0.1384	0.0094	0.0094	0.0017	−0.0013
yz-*xy*	0	0	0	0	0	0	0.0057	0
xz-*xy*	0	0	0	0	0	0	0.0057	0
yz-*yz*	−0.3224	−0.0389	−0.2914	0.0165	0.0010	0.0612	−0.0188	0.0006
yz-*xz*	0	0	0	−0.0121	0	0	−0.0136	0
xz-*xz*	−0.3224	−0.2914	−0.0389	0.0165	0.0612	0.0010	−0.0188	0.0006

TABLE II. Effective hopping parameters along the direction $[lmn]$ and on-site energy in eV associated to the t_{2g}-like Wannier functions for the $Sr_3Ru_2O_7$. The connecting vector is expressed in terms of the integer set $[l\ m\ n]$ and the lattice constants a and c as $\mathbf{d} = l\,a\,\mathbf{x} + m\,a\,\mathbf{y} + n\,c\,\mathbf{z}$ [28,37,55]. The direction $00p$ connect the two ruthenium atoms in the bilayer. The hopping parameters that are zero in the tetragonal phase have sign dependent from the tilting of the octahedra (clockwise or anticlockwise). The hopping parameters $t^{\frac{1}{2}\frac{1}{2}\frac{1}{2}}$ can have different connections: Depending on the character of the rotation of the two octahedra, the hopping parameter can increase, decrease, or be similar in amplitude to those obtained for the Sr_2RuO_4 compound.

Orbital index	Amplitude							
$[l\ m\ n]$	[000]	[100]	[010]	[110]	[200]	[020]	$\left[\frac{1}{2}\ \frac{1}{2}\ \frac{1}{2}\right]$	[00p]
xy-xy	−0.482	−0.292	−0.292	−0.134	−0.021	−0.021	0.002/0.001	−0.018
yz-xy	0	±0.001	±0.010	±0.001	±0.002	±0.006	0.006/0.005/0.004	0
xz-xy	0	±0.010	±0.001	±0.001	±0.006	±0.002	0.006/0.005/0.004	0
yz-yz	−0.386	−0.020	−0.301	0.014	0.002	0.041	−0.023/−0.018/−0.014	−0.264
yz-xz	0	±0.061	±0.061	−0.013	±0.007	±0.007	−0.024/−0.015/−0.006	0
xz-xz	−0.386	−0.301	−0.020	0.014	0.041	0.002	−0.023/−0.018/−0.014	−0.264

rotation of the octahedra slightly modifies their character by leading to a small charge redistribution following the distortion of the orthorhombic structure. In particular, this misalignment turns out to be more pronounced for the MLWFs, which has an orbital distribution with d_{xy} symmetry. Similar conclusions have been also reported in Ref. [61].

The effective electronic parameters based on the t_{2g}-like MLWFs are reported in Table II. There are different aspects that can be noticed when comparing the effective hopping of the Sr_2RuO_4 with those of the $Sr_3Ru_2O_7$. The first observation is that the nearest-neighbor hopping for the d_{xy} orbital in the distorted structural configuration is reduced with respect to the ideal tetragonal case and gets closer in amplitude with that one for the d_{xz} and d_{yz} states. The reduction for the hopping parameters between d_{xy} orbital can be also phrased in a Slater and Koster scheme [34]. For instance, the integral overlap E_{d_{xy},p_x} between the d_{xy} orbital on Ru and the $2p_x$ orbital on O reduces when there is a deviation of the Ru-O-Ru bond angle from 180°. Since the effective Ru-Ru hopping between the d_{xy} orbitals $t^{100}_{xy,xy}$ depends on the amplitude E_{d_{xy},p_x}, the reduction expected from the Slater and Koster approach is consistent with the result obtained within the MLWFs approach. As an indirect consequence of the change of the xy nearest-neighbor hopping, the VHS moves below the Fermi level, as shown in Fig. 3. Then one can note that the Ru-Ru hybridization via the d_{xy} orbital occurs both within the bilayer and also for the second nearest neighbor in the RuO_2 layers. The d_{xy} orbital exhibits also non-negligible overlap with the d_{xz} and d_{yz} within the RuO_2 layers. Such hybridization processes are identically zero by symmetry in the Sr_2RuO_4 system and thus represents a relevant contribution in the determination of the electronic structure and consequently the Fermi surface topology for the $Sr_3Ru_2O_7$. Concerning the c-axis dispersion, the γz orbitals have a larger overlap across the bilayers if compared to the Sr_2RuO_4 system.

Finally, looking at the structural analysis, from the Table III we find out that the a lattice constant almost coincides with the experimental value, while the experimental c lattice constant is slightly lower than the numerical value. Also in this case, the theoretical volume is ∼0.7% larger than the experimental one.

IV. $Sr_2RuO_4/Sr_3Ru_2O_7$ SUPERLATTICE: STRUCTURAL PROPERTIES

In this section we consider the structural properties of the $Sr_2RuO_4/Sr_3Ru_2O_7$ superlattices. The fully relaxed volume and the atomic positions have been determined for the two superlattice configurations, shown in Figs. 1(c) and 1(d), of the type $(Sr_2RuO_4)_l/(Sr_3Ru_2O_7)_m$ with $(l,m) = (3,3)$ and $(4,2)$, where l and m are the number of $n = 1$ and $n = 2$ unit cells in the heterostructure. Hereafter we denote as HET42 and HET33 the two superlattice structures with $(l,m) = (4,2)$ and $(3,3)$, respectively.

As a first outcome of the structural analysis, we have compared the lattice constants of the $n = 1$ and $n = 2$ bulk phases with the ones obtained by the full relaxation of the HET42 and HET33. The results are reported in Table III and include also the comparison with the experimental available data. When the HET42 and HET33 configurations are considered, we find that the HET42 in-plane lattice constant has an intermediate value between the amplitude of the Sr_2RuO_4 and $Sr_3Ru_2O_7$ bulk phases. Otherwise, for the case of the HET33 superlattice, where the number of $Sr_3Ru_2O_7$ cells is increased, a gets further reduced if compared to the theoretical values obtained for the pure Sr_2RuO_4 and $Sr_3Ru_2O_7$. Such modification of the in-plane lattice constants influences the dimension of the unit cell along the c axis, leading to an overall elongation. The difference of the lattice constant a between the HET42 and the HET33 system can be ascribed to the size mismatch

TABLE III. Comparison between the experimental data available and theoretical estimation of the lattice constants for the Sr_2RuO_4, $Sr_3Ru_2O_7$, and heterostructure. The length unit is in angstrom.

	Exp. Sr_2RuO_4 [54]	Th. Sr_2RuO_4	Exp. $Sr_3Ru_2O_7$ [60]	Th. $Sr_3Ru_2O_7$	$(Sr_2RuO_4)_4$-$(Sr_3Ru_2O_7)_2$	$(Sr_2RuO_4)_3$-$(Sr_3Ru_2O_7)_3$
a	3.862	3.887	3.873	3.872	3.881	3.869
c	12.723	12.650	20.796	20.968	46.234	50.554

TABLE IV. Inequivalent atomic bonds length in bulk ruthenates and for the $(Sr_2RuO_4)_4/(Sr_3Ru_2O_7)_2$ and $(Sr_2RuO_4)_3/(Sr_3Ru_2O_7)_3$ superlattices. The inner layers are the RuO_2 planes which have neighbors along the c axis having the same unit cell. For instance, in Fig. 4(b) they are labeled as B3 and B4 for the $Sr_3Ru_2O_7$ region and M2 for the Sr_2RuO_4 one. The interface layers are those at the boundary between the Sr_2RuO_4 and $Sr_3Ru_2O_7$ regions of the superlattice. In Fig. 4(b) they are denoted as B1 and B2 for the $Sr_3Ru_2O_7$ region, and M1 for the Sr_2RuO_4 one. There are empty spaces in the table because the corresponding values are not allowed for the given crystal structure.

	Exp. [54,60]	Th. Bulk	Inner layers HET42	Interface layers HET42	Inner layers HET33	Interface layers HET33
Ru-O_{ap} in Sr_2RuO_4	2.062	2.059	2.059	2.069	2.068	2.076
Ru-O_{ap} in $Sr_3Ru_2O_7$	2.038	2.059	2.058	2.050	2.063	2.056
Ru-O_{pl} in Sr_2RuO_4	1.931	1.943	1.943	1.943	1.934	1.934
Ru-O_{pl} in $Sr_3Ru_2O_7$	1.956	1.972	1.977	1.977	1.973	1.972
Ru-O_{in} in $Sr_3Ru_2O_7$	2.026	2.045	2.043	2.045	2.049	2.052
Sr-O_{ap} in Sr_2RuO_4 along c	2.429	2.433	2.433		2.431	
Sr-O_{ap} in $Sr_3Ru_2O_7$ along c	2.452	2.449	2.455		2.447	
$Sr^{(n=2)}$-$O_{ap}^{(n=1)}$ along c				2.423		2.416
$Sr^{(n=1)}$-$O_{ap}^{(n=2)}$ along c				2.472		2.469
Sr-O_{ap} in Sr_2RuO_4 in ab	2.738	2.757	2.757	2.758	2.745	2.747
Sr-O_{ap} in $Sr_3Ru_2O_7$ in ab	2.744	2.743	2.755	2.755	2.739	2.740
Sr-O_{pl} in Sr_2RuO_4	2.688	2.670	2.671	2.673	2.676	2.675
Sr-O_{pl} in $Sr_3Ru_2O_7$	2.506/2.896	2.473/3.002	2.478/2.997	2.480/2.997	2.470/3.015	2.473/3.017
Sr_{in}-O_{in}	2.738	2.738	2.747	2.747	2.737	2.736
Sr_{in}-O_{pl}	2.607/2.986	2.548/3.064	2.556/3.062	2.553/3.055	2.545/3.074	2.543/3.068

along the c axis between the $Sr_3Ru_2O_7$ and Sr_2RuO_4 phases in the two heterostructures. We attribute to this unbalance the origin of the obtained equilibrium structural configuration for the HET33 system where an elongation of the octahedra along the c axis occurs in the Sr_2RuO_4, accompanied by a reduction of the Ru-O distances in the plane with respect to the bulk values. The tendency to balance the c-axis length between the Sr_2RuO_4 and $Sr_3Ru_2O_7$ cells acts as an effective negative pressure on the Sr_2RuO_4 region in the c-axis direction which drives a shrinking of the in-plane lengths of the whole heterostructure. By an inspection of the Table IV, where we use the notation introduced in Fig. 4(a), one can note that for the $Sr_3Ru_2O_7$ region of the HET33 the elongation of the octahedra tends to compensate each other along the c axis. Indeed, for the $Sr_3Ru_2O_7$ units, in the inner layers the octahedra get elongated while at the $Sr_2RuO_4/Sr_3Ru_2O_7$ interface they are flattened. The net result is that there is a small deviation of the c-axis length of the $Sr_3Ru_2O_7$ block within the superlattice compared to the bulk. On the contrary, the octahedra in the Sr_2RuO_4 side of the HET33 superlattice gets completely elongated both for the inner and the interface layers. In particular, the distance between the Ru atom and the apical oxygen O_{ap} at the $Sr_2RuO_4/Sr_3Ru_2O_7$ interface is significantly larger than the corresponding amplitude in the Sr_2RuO_4 bulk. In the HET42 system the number of RuO_2 layers in the $n = 1$ and $n = 2$ side of the heterostructure is the same. This implies that there is no significant contribution due to the c-axis mismatch and, consequently, the main changes occur only as a consequence of the unbalance of the Ru-O planar distances. In this case, the positions that minimize the energy are obtained by an elongation in the plane of the $Sr_3Ru_2O_7$ and a consequent small shortening along the c axis. At the interface the matching is achieved by balancing the Ru-O_{ap} distances, i.e., the $Sr_3Ru_2O_7$ gets shorter and the Sr_2RuO_4 elongates. This result can be also understood because in the HET42 system the Sr_2RuO_4 region is more structurally stable since there are two units of inner layers that are not interfaced with the $Sr_3Ru_2O_7$ and, thus, have equilibrium positions very close to the Sr_2RuO_4 bulk system. Hence, the interior block of the Sr_2RuO_4 would tend to be more stable towards structural changes and would drive the structural modifications in the other layers of the superlattice. Such argument does not apply to the HET33 case because the number of the unit cells is the same and both the $n = 1$ and $n = 2$ subsystems have one block of RuO_2 inner layers and two interface layers. This aspect confirms the idea that the HET33 is more sensible to structural

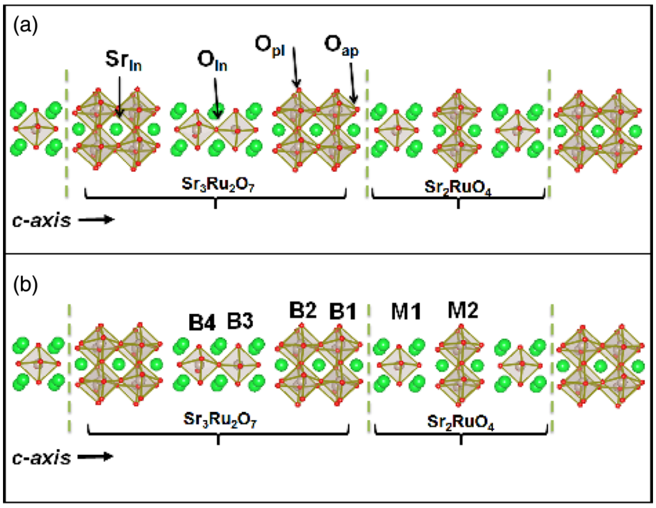

FIG. 4. (Color online) Notation about the labeling of the atoms (a) and of the layers (b) within the superlattice. O_{pl} is the planar oxygen, O_{ap} is the apical oxygen, O_{in} denotes the intrabilayer oxygen, and Sr_{in} the intrabilayer strontium. Sr_{in} and O_{in} are present only in the $Sr_3Ru_2O_7$ side of the heterostructure. The remaining strontium atoms are labeled Sr.

TABLE V. Ru-O-Ru bond angles and displacement of Ru in the several cases studied. At the interface, the modification of the Ru-O-Ru bond angle in Sr_2RuO_4 it is due to the Ru displacement along the c axis, no rotations are found.

	Exp. [54,60]	Th. Bulk	Inner RuO_2 layers HET42	Interface HET42	Inner RuO_2 layers HET33	Interface HET33
Δz in Sr_2RuO_4	0	0	0	0.008	0	0.007
Δz in $Sr_3Ru_2O_7$	0.017	0.033	0.032	0.039	0.030	0.037
Ru-O-Ru bond angle in Sr_2RuO_4	180.0°	180.0°	180.0°	179.5°	180.0°	179.6°
Ru-O-Ru bond angle in $Sr_3Ru_2O_7$	163.9°	158.1°	158.6°	158.8°	157.4°	157.5°

changes which can deviate from the Sr_2RuO_4 and $Sr_3Ru_2O_7$ bulk values. We expect that when the c-axis length of the $n = 1$ and $n = 2$ regions are comparable, it is the subsystems with a larger number of unit cells that should control the change of the structural configuration. We would like also to point out that the $Sr_3Ru_2O_7$ bulk system exhibitshas an orthorhombic symmetry and can better account for a reduction of the in-plane lattice parameters by suitably rotating the RuO_6 octahedra. Such degree of freedom is energetically unfavorable when the Sr_2RuO_4 is considered since its stability in a tetragonal symmetry poses a constraint to possible deformations of the crystal structure. As a final consideration, we note that the bond lengths involving the Sr atoms and the surrounding oxygens are also modified in the superlattice compared to the bulk phases. The relevant changes are observed at the interface where there are two Sr-O_{ap} bonds along c: the first between the Sr of the $n = 2$ phase and the O_{ap} of the $n = 1$ phase, the second between the Sr of the $n = 1$ phase and the O_{ap} of the $n = 2$, and the first bond decreases, while the second one increases with respect to the bulk and inner layer values.

To complete the structural analysis, we have studied the Δz displacement along the c axis of the Ru atoms with respect to the planar oxygens and the variation of the Ru-O-Ru bond angles. The results are summarized in Table V, from which we can infer two different trends for Δz in Sr_2RuO_4 and $Sr_3Ru_2O_7$. Indeed, as far as Δz for Sr_2RuO_4 is considered, we see that in the inner region of both the HET42 and HET33 structures this quantity is zero, i.e., there is no variation of the displacement along the c axis of Ru ions compared to the pure phase. On the other hand, at the interface a small Δz is produced and the Ru atom goes far from the interface as shown in Fig. 5. Concerning the $Sr_3Ru_2O_7$, a Δz is already present in the case of the bulk phase, but an enhancement of the amplitude of Δz is deduced at the interface.

Referring to the Ru-O-Ru bond angles, there is no significant variation in the inner layers of the Sr_2RuO_4 side of the superlattice for both the HET42 and HET33 configurations, while at the interface the displacement along the c axis of the Ru atoms produces a reduction of the Ru-O-Ru bond angle. The situation differs completely for the $Sr_3Ru_2O_7$ side of the hybrid structure. Indeed, a deviation from the pure phase angle is found, as well as in the inner region, exhibiting a dependence whose amplitude is related to the size of considered superlattice. However, the bond angle increases with respect to the inner region in both cases. The rotation angle of the octahedra, which is half of the supplementary of the Ru-O-Ru bond angle, decreases at the interface in the $Sr_3Ru_2O_7$ phase.

On the basis of the results above discussed the picture that emerges is shown in Fig. 5. The change of the atomic positions reveals a tendency of the ions positively charged in the ionic picture to move in the direction of the Sr_2RuO_4 side, while the negative ones go in the opposite direction towards the $Sr_3Ru_2O_7$ side. We note that two bonds are strongly modified at the interface: the distance between the ruthenium and the apical oxygen and the distance between the Sr ion and the apical oxygen along the c axis, the other in-plane modifications being smaller. At the interface between Sr_2RuO_4 and $Sr_3Ru_2O_7$, two different SrO insulator planes meet. The different geometrical configurations of SrO planes make near the Sr of the $n = 2$ phase and the O_{ap} of the $n = 1$ phase, so a new bond not present in the bulk is created, and this new bond may drive the interface reconstruction shown in Fig. 5.

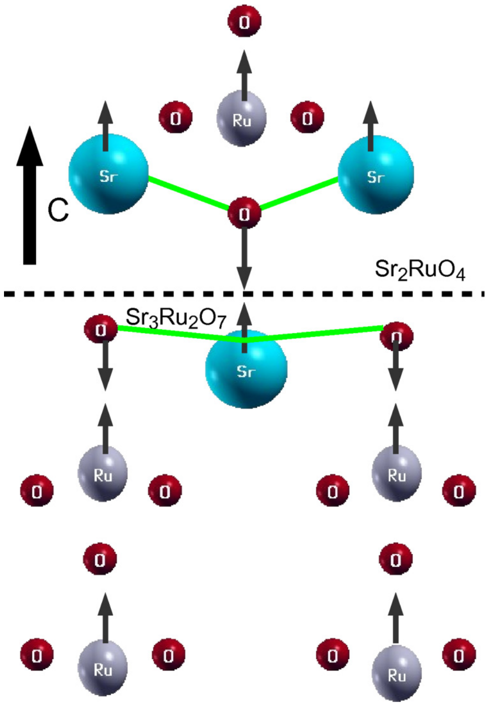

FIG. 5. (Color online) Schematic view of the atomic rearrangement at the interface of the $Sr_2RuO_4/Sr_3Ru_2O_7$ heterostructure, observed in both HET42 and HET33. The arrows indicate the most relevant displacements at the interface as compared to the bulk and inner layers. The different geometrical configuration of the SrO plane is shown (green line). It is more flat for $Sr_3Ru_2O_7$, while there is a greater difference between the Sr and the O atom along the c axis in Sr_2RuO_4. The SrO planes are altered at the interface.

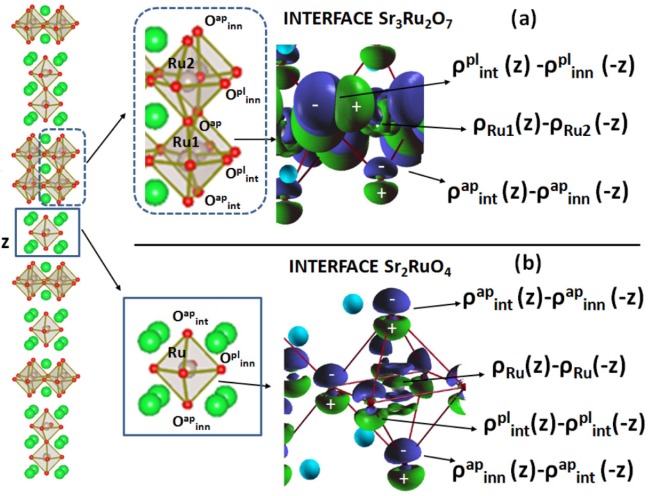

FIG. 6. (Color online) Differences between the electron density for the $(Sr_2RuO_4)_3/(Sr_3Ru_2O_7)_3$ superlattice for the $Sr_3Ru_2O_7$ (a) and Sr_2RuO_4 (b) sides of the interface.

To clarify the consequences of the symmetry breaking and the structural reconstruction due to the $Sr_2RuO_4/Sr_3Ru_2O_7$ interface, we have determined the differences of the electronic distribution, as given by the first-principles calculations, by comparing those associated with the atoms placed close to the Sr_2RuO_4-$Sr_3Ru_2O_7$ interface and those that are in the inner layers within the Sr_2RuO_4 and $Sr_3Ru_2O_7$ regions of the heterostructure. The analysis is performed to single out how the structural modifications of the Sr-O and Ru-O bonds affect the electronic distribution. Although the results refer to the HET33, they are also qualitatively representative of the HET42 system. To discuss the outcomes, it is useful to introduce the total electron density distribution $\rho_{\alpha}^{\beta}(\mathbf{r})$ at a given position $\mathbf{r}$ for the atom β (with β indicating the ruthenium, the apical ap, or the planar pl oxygen atom) belonging to the α RuO_2 layers, α being the the inner (inn) or the interface (int) layer. The results, presented in the Fig. 6, show that the differences between the interface and the inner layers electronic distribution depend on the selected region of the heterostructure. For the Sr_2RuO_4 side, if we compare the apical oxygen pointing towards the interface with that to the inner layers, the difference indicates that the electron density gets reduced in the part where the O is bonding with the Sr in the $Sr_3Ru_2O_7$ phase. Otherwise, there is an increase of charge along the bond between the apical oxygen and the Ru for the one close to the interface, i.e., the Ru-O^{ap}_{int}, if compared with the Ru-O^{ap}_{inn} bond, which is near the inner layer of the Sr_2RuO_4 region. This result is consistent with the modification of the Sr-O bonds close to the interface, as shown in Fig. 5. Indeed, the apical oxygen O^{ap}_{int} in the Sr_2RuO_4 region at the interface tends to reduce the Sr-O bond length and, accordingly, leads to an increase of the distance with the Ru compared to the apical oxygen O^{ap}_{int} which is near the Sr_2RuO_4 inner layers. The observed electronic redistribution originates from the nature of the Ru-O ligand. A small modification of the electron density is also obtained at the Ru site. To investigate these variations, we have determined the difference between the electron density along the bond Ru-O^{ap}_{int} directed towards the interface and the one for the bond Ru-O^{ap}_{inn} pointing to the inner layers (see Fig. 6). Furthermore, for the ruthenium electron density there is a slight reduction of charge close to the oxygen than to the ruthenium atom in the longer bond, i.e., Ru-O^{ap}_{int} ($z > 0$), compared to the shorter Ru-O^{ap}_{inn}. We note that the charge asymmetry is basically isotropic in the plane because there are no significant effects due to the planar oxygens. When the $Sr_3Ru_2O_7$ region of the heterostructure is considered, we have focused the attention on the differences emerging between the two octahedra, forming the $Sr_3Ru_2O_7$ bilayered cell, which are placed near the interface and the inner layers. For the apical oxygens the differences are analogous to the Sr_2RuO_4 case with an asymmetry due to the long and short Ru-O_a bonds. The structural change close to the interface leads to a variation of the electron density at the ruthenium site for the two ruthenium atoms in the bilayer. For the ruthenium atoms, we compare the electron density along the bond Ru1-O^{ap}_{int} and the one for the bond Ru2-O^{ap}_{int} as well as the distributions associated with the corner sharing oxygens between the octahedra in the bilayer, i.e., Ru1-O_a and Ru2-O_a (see Fig. 6). For the planar oxygens, the variation in the electronic density among the atoms close to the interface (O^{pl}_{int}) and those in the inner side (O^{pl}_{inn}) shows a reconstruction in the *ab* plane along the Ru-O bond and perpendicular to it. The result is a peculiar angular dependence of the difference in the electronic density. The origin of such variation within the bilayer arises mainly from the differences in the Ru-O-Ru bond angle and in the shift of the Ru1 and Ru2 positions within the bilayer.

V. $Sr_2RuO_4/Sr_3Ru_2O_7$ SUPERLATTICE: ELECTRONIC PROPERTIES

We have determined the electronic properties of HET42 and HET33 heterostructures with the aim to analyze the modifications of the spectra within the superlattice and in comparison with the bulk phases as well as to extract the interrelation between the structural changes and the electronic dispersions. Based on the detailed analysis of the structural properties, we expect that the effective hopping and the hybridization parameters for the energy bands at the Fermi level are influenced both in the amplitude and in the character. Moreover, a rearrangement of the on-site Ru 4*d* energies is expected to influence the 4*d* energy splitting due to the flattening and elongation of the RuO_6 octahedra within the superlattice.

Since the unit cell is quite complex, we have analyzed the projected density of states for the Ru t_{2g}-like orbitals at the inner and the interface layers of the Sr_2RuO_4 and $Sr_3Ru_2O_7$ sides within the superlattice. Furthermore, in order to extract the relevant changes induced by the interface reconstruction and the structural distortions we have determined the effective tight-binding Hamiltonian in the MLWFs basis for the bands close to the Fermi level.

The results are presented only for the HET42 configuration, since we have checked that the HET33 structure does not exhibit substantial qualitative differences. In Fig. 7 it is reported the DOS for the projected t_{2g}-like bands of Ru atoms placed at the interface and inner layers for the Sr_2RuO_4 and $Sr_3Ru_2O_7$ side of the superlattice for an energy window close to the Fermi level where the major changes occur.

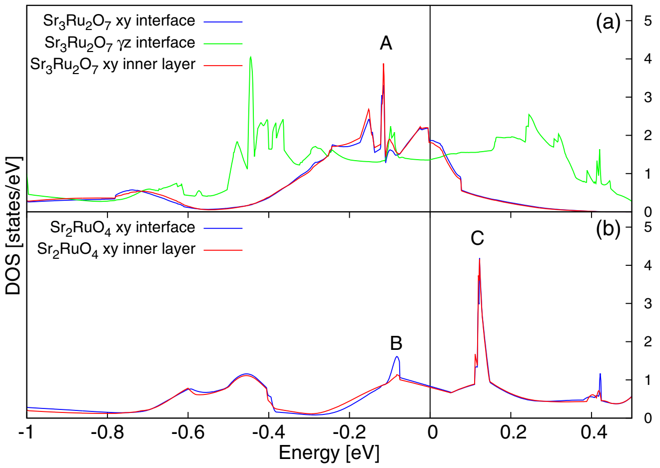

FIG. 7. (Color online) Projected density of states for the $4d$ bands of the Ru atoms placed at different layers within the HET42 heterostructure for the $Sr_3Ru_2O_7$ (top panel) and Sr_2RuO_4 (bottom panel) sides. The blue line represents the d_{xy} DOS for Ru atoms at the interface, and the red lines the DOS in the inner layers. A and C denote the position of the VHS and B corresponds to a peak appearing in the d_{xy} Sr_2RuO_4 DOS at the interface. The Fermi energy is set to zero.

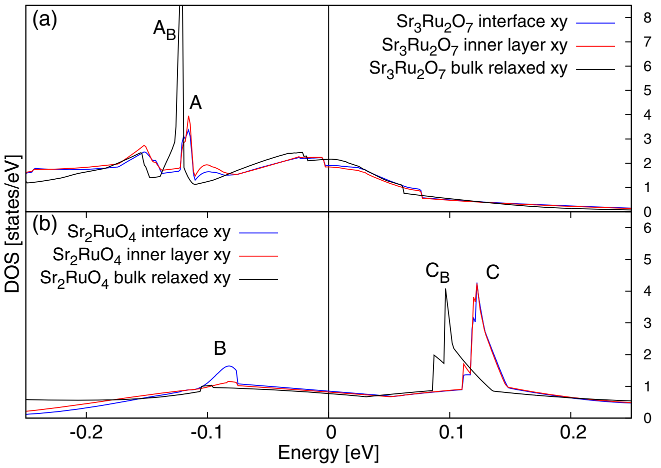

FIG. 8. (Color online) Bulk vs heterostructure projected density of states for the Ru xy band, near the Fermi level, for the $Sr_3Ru_2O_7$ (a) and Sr_2RuO_4 (b). A_B and C_B denote the position of the VHS in the bulk $Sr_3Ru_2O_7$ and Sr_2RuO_4, respectively, whereas A and C correspond to the position of the VHS in the superlattice. B indicates the peak appearing in the d_{xy} Sr_2RuO_4 DOS at the interface. The Fermi energy is set to zero.

From a general point of view, the DOS shows the features of the bulk Sr_2RuO_4 and $Sr_3Ru_2O_7$, for instance, as far as it concerns the van Hove–like peaks below (denoted by A) and above the Fermi level (denoted by C) for the d_{xy} bands and the one-dimensional distribution of spectral weight for the γz ones. It is worth stressing that, though the octahedra deformation is not uniform within the superlattice, the DOS does not exhibit significant shifts in energy when comparing the interface with the inner layers. This can be addressed by considering that the change in the crystal field and the modification of the effective bandwidth can balance and reduce the energy shifts within the superlattice. According to the crystal field theory, the Coulomb potential generated by the point charge distribution of the oxygens around the ruthenium atom leads to a removal of the energy degeneracy between the t_{2g} manifold. Similar effects are also due to the formation of a covalent bonding by the Ru($4d$) and the O($2p$) states. Depending on the character of the octahedra, being flatten (elongated), the energy associated with the d_{xy} Wannier state can be higher (lower) than that of the d_{xz} or d_{yz} ones. On the other hand, the rotation of the octahedra provides a removal of the energy degeneracy between the d_{xz} and d_{yz} Wannier states in the form of a splitting, for octahedral rotation around the a or b in-plane crystal axes, or mixing/hybridization, for an octahedral rotation around the c axis. The analysis of the effective tight-binding parameters within the MLWFs reveal that indeed this is the case for the $Sr_2RuO_4/Sr_3Ru_2O_7$ heterostructure.

Slight changes are visible only for the d_{xy} bands, whereas in the $Sr_3Ru_2O_7$ there is a small suppression of spectral weight below the Fermi level at the interface compared to the inner layers; the opposite occurs above the Fermi energy. The Ru d_{xy} DOS in the Sr_2RuO_4 side of the superlattice exhibits a slight increase of the spectral weight (peak B in the Fig. 7) at energies where a redistribution and an overlap of the $d_{\gamma z}$ bands with the d_{xy} one occur in the $Sr_3Ru_2O_7$ region. No significant variations can be noticed for the γz bands across the superlattice.

More interesting is the comparison between the DOS of the superlattice and of the bulk Sr_2RuO_4 and $Sr_3Ru_2O_7$ systems. We focus on the variation of the VHS positions close to the Fermi level for the xy band. In Fig. 8 we present the d_{xy} DOS for the interface and inner layers of the HET42 superlattice for the Sr_2RuO_4 and $Sr_3Ru_2O_7$ sides in comparison with the corresponding bulk DOS. We note that the peak associated with the VHS in the bulk $Sr_3Ru_2O_7$ gets reduced and shifted towards the Fermi level in the $Sr_3Ru_2O_7$. This is mainly due to the change of the d_{xy} bandwidth and of the crystal field splitting driven by the rotation and flattening or elongation of the octahedra. On the other hand, the VHS placed above the Fermi level in the Sr_2RuO_4 is moved away from the Fermi level.

We point out that the position and the intensity of the VHS depend essentially on two parameters, the energy on-site and the effective electronic parameters related to the Ru-Ru hopping amplitudes, and it is strictly related to the character of the momentum dispersion around the VHS point. In our case, we recall that this singularity is located within the d_{xy} band. To understand the origin of the shift between the VHS for the Sr_2RuO_4 we use the following approximated expression for the dispersion of the d_{xy} band:

$$\varepsilon_{xy}(\mathbf{k}) \approx \varepsilon^0_{xy} + t^{100}_{xy,xy}(\cos(ak_x) + \cos(ak_y)) + 4t^{110}_{xy,xy}\cos(ak_x)\cos(ak_y),$$

where the chemical potential is set to zero. In this expression we have neglected terms which are smaller in amplitude as related to the hybridization between the xy and the γz bands and to the hopping processes of higher order than the second nearest neighbors. Considering that the Sr_2RuO_4 VHS is placed at the point $(0,\pi)$ or $(\pi,0)$ of the Brillouin zone, the energy of the VHS ε_{VHS} is given by

$$\varepsilon_{\text{VHS}} \approx \varepsilon^0_{xy} + 4\left|t^{110}_{xy,xy}\right|,$$

where ε^0_{xy} depends on the crystal field and $|t^{110}_{xy,xy}|$ is inversely proportional to a power of the lattice constant a and directly proportional to a power of the the cosine of the rotation angle [34]. For instance, at the interface of the heterostructure in the Sr_2RuO_4 side there is a reduction of the hopping parameter with respect to the inner layer, but the variation of the crystal field tends to balance this effect reducing the difference of the ε_{VHS} between the interface and the inner layer. We may also estimate the shift of the VHS energies by comparing the bulk and the superlattice parameters. Hence, in the Sr_2RuO_4 case, the reduction of a in the heterostructure increases $|t^{110}_{xy,xy}|$ and, subsequently, ε_{VHS}. On the contrary, for the bilayer compound the superlattice VHS singularity is closer to Fermi level than in the bulk $Sr_3Ru_2O_7$. This is mainly due to the change of the d_{xy} bandwidth and of the crystal field splitting driven by the rotation and flattening or elongation of the octahedra. Concerning the intensity, the reduction of the peak for the superlattice is related to the modification of the dispersion around the point which in turn originates from the reduced symmetries of the allowed hopping amplitudes in the superlattice structure.

Let us comment on the connection between these results and possible experimental consequences. A first potential link derives from the modification of the density of states close to the Fermi energy. The resulting DOS for the Ru xy band at the interface in the Sr_2RuO_4 side of the superlattice turns out to be greater than that in the uniform Sr_2RuO_4. Hence, the reduction of the bandwidth of the Ru xy band in the superlattice would point towards an enhancement of the correlations at the interface. These feature indicate a tendency toward the increase of the superconducting critical temperature either viewed in a Bardeen-Cooper-Schrieffer scenario or in a correlated driven pairing. Furthermore, the growth of the DOS at the Fermi level and the change in the effective bandwidth may also lead to a ferromagnetic instability within a Stoner picture supporting the possibility that the superlattice could exhibit a ferromagnetic transition. Nowadays the only reproducible eutectic system so far available, i.e., the $Sr_2RuO_4/Sr_3Ru_2O_7$ system [18] may offer the opportunity to analyze and compare the effects of the interfacing between the first two RP members. Electric transport and muon spin measurements in this eutectic compound confirm the occurrence of superconductivity at a critical temperature higher than that observed in the *pure* Sr_2RuO_4, with an onset of about 2.5 K whose origin could be ascribed to the $Sr_2RuO_4/Sr_3Ru_2O_7$ interface [21]. Our study would support such a scenario though an analysis of the pairing strength at the interface is required to further understand how the superconductivity is modified at the boundary.

Starting from the outcome of the density functional analysis and to understand more deeply the differences in the electronic properties within the superlattice and with respect to the bulk Sr_2RuO_4 and $Sr_3Ru_2O_7$, we have determined the effective tight-binding Hamiltonian in the MLWFs basis. The output of the relevant electronic parameters connecting the Ru t_{2g}-like Wannier states is given in Table VI for the case of the HET33 heterostructure. This is the more general case, as it contains inequivalent inner RuO_2 layers for both the Sr_2RuO_4 and $Sr_3Ru_2O_7$ subsystems. Starting from the $Sr_3Ru_2O_7$ side of the heterostructure, we note that the electronic parameters are quite homogeneous within the superlattice, confirming the small variations in the DOS at the interface and in the inner RuO_2 layers. In particular, the small modification of the local crystal field splitting, the bilayer splitting, and the t_{2g} bandwidth have a trend that follows the main structural changes. Indeed, since the octahedra are flattened for the outer RuO_2 layers at the interface [denoted as B1 and B2 in Fig. 4(b)] with respect to those in the inner layers [denoted as B3 and B4 in Fig. 4(b)] the energy associated to the d_{yz}-like Wannier states is pushed up while the d_{xy} is not modified. Thus, the overall effect is to reduce the crystal field splitting, i.e., $\Delta_{cf} = |\varepsilon^0_{xy} - \varepsilon^0_{yz}|$, at the interface with respect to the $Sr_3Ru_2O_7$ inner side of the superlattice. On the other hand, the bilayer splitting, the t_{2g} in-plane and out-of-plane nearest-neighbor hopping are basically uniform within the superlattice, exhibiting a variation in an energy window of 2–10 meV. In such an energy range the most significant modification is represented by the increase of the Ru-Ru yz nearest-neighbor hopping when moving from the interface to the inner layers. It is also worth noting that the hybridization amplitude between the xy and yz Wannier states is larger in the RuO_2 layers at the interface with the Sr_2RuO_4 than in the inner ones. At this point, it is also relevant to analyze the differences of the effective tight-binding Hamiltonian between the superlattice $Sr_3Ru_2O_7$ side and the corresponding bulk phase. By inspection of Table II we note that, due to a larger tilting of the octahedra with respect to the bulk, the in-plane xy Ru-Ru nearest-neighbor hopping is reduced in the superlattice. There occurs also a decrease of the yz Ru-Ru nearest-neighbor hopping but this is mainly driven by the flattening of the RuO_6 octahedra in the superlattice. The distortion of the octahedra influences also the crystal field and the bilayer splitting. The energy splitting Δ_{cf} is generally reduced in the superlattice if compared to the bulk phase except for the Ru atoms placed in the B1 outer layer of the interface bilayer [see Fig. 4(b)]. The hybridization amplitude between the xy and yz Wannier states, which is a relevant parameter in setting the differences between the Sr_2RuO_4 and $Sr_3Ru_2O_7$ electronic structures, is doubled at the interface of the superlattice compared to that for the $Sr_3Ru_2O_7$ bulk phase.

Let us consider the electronic parameters for the Sr_2RuO_4 bulk and in the superlattice. Starting from the crystal field splitting we note that the elongation of the octahedra at the interface pushes down the energy of the Ru yz states. Such a change, in turn, leads also to an increase of the Ru-Ru in-plane nearest-neighbor hopping moving from the inner layers to the interface ones. The remaining tight-binding parameters keep the symmetry connections as in the Sr_2RuO_4 bulk phase. Though the presence of a structural rearrangement at the $Sr_2RuO_4/Sr_3Ru_2O_7$ interface leads to flattening and rotation of the octahedra there are no extra induced hybridizations between the t_{2g}-like Wannier states. The comparison of the effective tight-binding Hamiltonian between the Sr_2RuO_4 side of the superlattice and the corresponding bulk phase shows that the in-plane xy Ru-Ru nearest-neighbor hopping is slightly reduced in the superlattice and the same happens to the yz orbitals. Hence, apart from a renormalization of the t_{2g}

TABLE VI. Effective hopping parameters along the direction $[lmn]$ and on-site energy in eV associated to the t_{2g}-like Wannier functions for the $(Sr_2RuO_4)_3/(Sr_3Ru_2O_7)_3$ superlattice. The connecting vector is expressed in terms of the integer set $[l\ m\ n]$ and the lattice constants a and c as $\mathbf{d} = l\,a\,\mathbf{x} + m\,a\,\mathbf{y} + n\,c\,\mathbf{z}$ for the related subsystems. The direction $00p$ connect the two ruthenium atoms within the bilayer of the $Sr_3Ru_2O_7$ side of the superlattice. B1 and B2 indicate the RuO_2 layers within the bilayer placed at the interface with the Sr_2RuO_4 and the $Sr_3Ru_2O_7$ side of the superlattice. B3 and B4 are the inner RuO_2 layers in the $Sr_3Ru_2O_7$ part. M1 and M2 indicate the interface and the inner RuO_2 layers within the Sr_2RuO_4 side. A schematic view of the structure and the labels is reported in Fig. 4(b).

	$Sr_3Ru_2O_7$									Interface	Sr_2RuO_4				
Orbital	B4-B3	B3		B3-B2	B2		B2-B1	B1		B1-M1	M1		M1-M2	M2	
$[l\ m\ n]$	[00p]	[000]	[100]	$\left[\frac{1}{2}\ \frac{1}{2}\ \frac{1}{2}\right]$	[000]	[100]	[00p]	[000]	[100]	$\left[\frac{1}{2}\ \frac{1}{2}\ \frac{1}{2}\right]$	[000]	[100]	$\left[\frac{1}{2}\ \frac{1}{2}\ \frac{1}{2}\right]$	[000]	[100]
xy-xy	−0.015	−0.423	−0.235	0.002/0.001	−0.423	−0.235	−0.016	−0.424	−0.237	0.002	−0.490	−0.380	0.002	−0.491	−0.381
yz-xy	0	0	±0.001	0.006/0.004/0.003	0	±0.001	0	0	±0.001	0.006/0.005	0	± 0.001	0.006	0	0
xz-xy	0	0	±0.016	0.006/0.004/0.003	0	±0.016	0	0	±0.020	0.006/0.005	0	0	0.006	0	0
yz-yz	−0.248	−0.335	−0.008	−0.023/−0.015/−0.011	−0.332	−0.008	−0.244	−0.315	−0.008	−0.021/−0.014	−0.307	−0.039	−0.020	−0.289	−0.039
yz-xz	0	0	±0.080	−0.025/−0.013/−0.003	0	±0.079	0	0	±0.077	−0.020/−0.009	0	0	−0.015	0	0
xz-xz	−0.248	−0.335	−0.285	−0.023/−0.015/−0.011	−0.332	−0.285	−0.244	−0.315	−0.277	−0.021/−0.014	−0.307	−0.280	−0.020	−0.289	−0.273

bandwidth and a modification of the crystal field, splitting the electronic structure in the Sr_2RuO_4 keeps its qualitative features as far as it concerns, for instance, the nesting and the presence of the VHSs. We can also observe how the change of the xy nearest-neighbor hopping $t^{100}_{xy,xy}$ at the interface can be understood via the Ru-O-Ru bond angle. Indeed, the Ru-O-Ru angle at interface decreases for Sr_2RuO_4 and increases for Sr_2RuO_4 (Table V), consequently, the $t^{100}_{xy,xy}$ decreases for Sr_2RuO_4 and increases for Sr_2RuO_4 with respect to the inner layers values. Finally, we note that the broken mirror symmetry at the Sr_2RuO_4 interface induces a hybridization between the d_{xy} and d_{yz} orbitals in the [100] direction, as can be inferred from an inspection of Table VI. We mention that this modification of the electronic structure in the presence of the atomic spin-orbit coupling has been proved to play an important role in the spin-triplet pairing state near the surface/interface of Sr_2RuO_4 [62].

VI. CONCLUSIONS

By means of first-principles density functional theory we determined the structural and electronic properties of different configurations of superlattices made with Sr_2RuO_4 and $Sr_3Ru_2O_7$ compounds. In order to compare the relevant electronic parameters that determine the dispersions of the t_{2g}-like states close to the Fermi level, we have built up an effective tight-binding Hamiltonian in the MLWFs basis.

We have shown that, due to the different symmetry and size of the $n = 1$ and $n = 2$ elements, a rearrangement of the atomic position takes place within both the RuO_2 and SrO layers. The RuO_6 octahedra at the $Sr_2RuO_4/Sr_3Ru_2O_7$ interface get elongated in the Sr_2RuO_4 side and flattened in the $Sr_3Ru_2O_7$ along the c axis when compared to the octahedra in the inner layers block and those in the bulk phases as well. Another interesting feature is the observation of the change of misalignment of Sr atoms with respect to the O atoms in the SrO blocks at the $Sr_2RuO_4/Sr_3Ru_2O_7$ interface. The effect is not symmetric in amplitude on the two sides of the superlattice at the interface. Furthermore, we have demonstrated that similar structural changes occur also in the RuO_2 layers close to the interface and that they influence the Ru-O-Ru bond angle, resulting into a less pronounced rotation of the $Sr_3Ru_2O_7$ octahedra and a displacement of the Ru atom with respect to the oxygen plane in the Sr_2RuO_4 side of the interface.

Concerning the electronic structure, we find out that the superlattice electronic parameters are quite uniform and exhibit small differences between the interface and inner Ru bands. Furthermore, the symmetry allowed hopping in the superlattice are analog to those in the Sr_2RuO_4 and $Sr_3Ru_2O_7$ bulk phases with the major changes occurring in the modification of the amplitude of the electronic processes. For instance, this implies that the nesting of the γz is not affected qualitatively in the Sr_2RuO_4 side as well as the presence and the character of the VHSs. Otherwise, effects of the enhanced hybridization between the $n = 1$ and $n = 2$ bands and of the overall changes in the hopping amplitude manifest as shifts in the VHSs or transfer of spectral weights close to the Fermi level. The only exception is the Sr_2RuO_4 at the interface, where the displacement of the Ru atoms breaks the mirror symmetry respect to the RuO_2 plane allowing for the hybridization between the xy and γz bands.

Regarding the $Sr_3Ru_2O_7$ side, we have shown that the VHS is shifted towards the Fermi level in the superlattice if compared to the bulk phase. The closeness of the VHS to the Fermi energy is known to lead to a reduction of the metamagnetic critical field if analyzed in the framework of a weakly correlated approach for the metamagnetic instability [63]. Such a hypothesis can be experimentally tested and indirectly used to understand the origin of the metamagnetism in the $Sr_3Ru_2O_7$ with respect to the presence of the VHS. We finally note that the study of the physical properties of the superlattice or heterostructures involving $Sr_2RuO_4/Sr_3Ru_2O_7$ interfaces may represent a useful basis to explore the relevant mechanisms that determine the collective quantum behavior as well as the response upon an applied magnetic field.

ACKNOWLEDGMENTS

We acknowledge useful discussions with G. Cantele and E. Pavarini. C.A. acknowledges financial support from "Fondazione Angelo Della Riccia." The research leading to these results has received funding from the EU-FP7/2007-2013 under Grant No. 264098-MAMA.

[1] H. Y. Hwang, Y. Iwasa, M. Kawasaki, B. Keimer, N. Nagaosa, and Y. Tokura, Nat. Mat. **11**, 103 (2012).

[2] M. Imada, A. Fujimori, and Y. Tokura, Rev. Mod. Phys. **70**, 1039 (1998).

[3] J. Heber, Nature **459**, 28 (2009).

[4] A. Ohtomo, D. A. Muller, J. L. Grazul, and H. Y. Hwang, Nature **419**, 378 (2002).

[5] A. Gozar, Nature **455**, 782 (2008).

[6] A. Ohtomo and H. Y. Hwang, Nature **427**, 423 (2004).

[7] N. Nakagawa, H. Y. Hwang, and D. A. Muller, Nat. Mater. **5**, 204 (2006).

[8] Y. Tokura and H. Y. Hwang, Nat. Mater. **7**, 694 (2008).

[9] E. Dagotto, Science **318**, 1076 (2007).

[10] Y. Maeno, H. Hashimoto, K. Yoshida, S. Nishizaki, T. Fujita, J. G. Bednorz, and F. Lichtenberg, Nature **372**, 532 (1994).

[11] S.-I. Ikeda, Y. Maeno, S. Nakatsuji, M. Kosaka, and Y. Uwatoko, Phys. Rev. B **62**, R6089 (2000).

[12] R. S. Perry, L. M. Galvin, S. A. Grigera, L. Capogna, A. J. Schofield, A. P. Mackenzie, M. Chiao, S. R. Julian, S. I. Ikeda, S. Nakatsuji, Y. Maeno, and C. Pfleiderer, Phys. Rev. Lett. **86**, 2661 (2001).

[13] S. A. Grigera, R. S. Perry, A. J. Schofield, M. Chiao, S. R. Julian, G. G. Lonzarich, S. I. Ikeda, Y. Maeno, A. J. Millis, and A. P. Mackenzie, Science **294**, 329 (2001).

[14] G. Cao, L. Balicas, W. H. Song, Y. P. Sun, Y. Xin, V. A. Bondarenko, J. W. Brill, S. Parkin, and X. N. Lin, Phys. Rev. B **68**, 174409 (2003).

[15] Z. Q. Mao, M. Zhou, J. Hooper, V. Golub, and C. J. O'Connor, Phys. Rev. Lett. **96**, 077205 (2006).

[16] R. Gupta, M. Kim, H. Barath, S. L. Cooper, and G. Cao, Phys. Rev. Lett. **96**, 067004 (2006).

[17] P. B. Allen, H. Berger, O. Chauvet, L. Forro, T. Jarlborg, A. Junod, B. Revaz, and G. Santi, Phys. Rev. B **53**, 4393 (1996).

[18] R. Fittipaldi, A. Vecchione, S. Fusanobori, K. Takizawa, H. Yaguchi, J. Hooper, R. S. Perry, and Y. Maeno, J. Cryst. Growth **282**, 152 (2005).

[19] R. Ciancio, H. Petterson, J. Börjesson, S. Lopatin, R. Fittipaldi, A. Vecchione, S. Kittaka, Y. Maeno, S. Pace, and E. Olsson, Appl. Phys. Lett. **95**, 142507 (2009).

[20] R. Fittipaldi, D. Sisti, A. Vecchione, and S. Pace, Cryst. Growth Des. **7**, 2495 (2007).

[21] T. Shiroka, R. Fittipaldi, M. Cuoco, R. De Renzi, Y. Maeno, R. J. Lycett, S. Ramos, E. M. Forgan, C. Baines, A. Rost, V. Granata, and A. Vecchione, Phys. Rev. B **85**, 134527 (2012).

[22] J. Hooper, M. Zhou, Z. Q. Mao, Y. Liu, R. S. Perry, and Y. Maeno, Phys. Rev. B **73**, 132510 (2006).

[23] R. Fittipaldi, A. Vecchione, R. Ciancio, S. Pace, M. Cuoco, D. Stornaiuolo, D. Born, F. Tafuri, E. Olsson, S. Kittaka, H. Yaguchi, and Y. Maeno, Europhys. Lett. **83**, 27007 (2008).

[24] M. A. Zurbuchen, Y. Jia, S. Knapp, A. H. Carim, D. G. Schlom, L. Zou, and Y. Liu, Appl. Phys. Lett. **78**, 2351 (2001); M. A. Zurbuchen, Y. Jia, S. Knapp, A. H. Carim, D. G. Schlom, and X. Q. Pan, *ibid.* **83**, 3891 (2003).

[25] W. Tian, J. H. Haeni, D. G. Schlom, E. Hutchinson, B. L. Sheu, M. M. Rosario, P. Schiffer, Y. Liu, M. A. Zurbuchen, and X. Q. Pan, Appl. Phys. Lett. **90**, 022507 (2007).

[26] Y. Krockenberger *et al.*, Appl. Phys. Lett. **97**, 082502 (2010).

[27] P. Hohenberg and W. Kohn, Phys. Rev. **136**, B864 (1964); W. Kohn and L. J. Sham, *ibid.* **140**, A1133 (1965).

[28] X. Gonze, G. M. Rignanese, M. Verstraete, J. M. Beuken, Y. Pouillon, R. Caracas, F. Jollet, M. Torrent, G. Zerah, M. Mikami, P. Ghosez, M. Veithen, J. Y. Raty, V. Olevano, F. Bruneval, L. Reining, R. Godby, G. Onida, D. R. Hamann, and D. C. Allan, Zeit. Kristallogr. **220**, 558 (2005).

[29] Z. Wu and R. E. Cohen, Phys. Rev. B **73**, 235116 (2006).

[30] M. Fuchs and M. Scheffler, Comput. Phys. Commun. **119**, 67 (1999).

[31] N. Marzari, D. Vanderbilt, A. De Vita, and M. C. Payne, Phys. Rev. Lett. **82**, 3296 (1999).

[32] D. I. Bilc, R. Orlando, R. Shaltaf, G.-M. Rignanese, J. Iñiguez, and P. Ghosez, Phys. Rev. B **77**, 165107 (2008).

[33] J. P. Perdew, K. Burke, and M. Ernzerhof, Phys. Rev. Lett. **77**, 3865 (1996).

[34] J. C. Slater and G. F. Koster, Phys. Rev. **94**, 1498 (1954).

[35] N. Marzari and D. Vanderbilt, Phys. Rev. B **56**, 12847 (1997).

[36] I. Souza, N. Marzari, and D. Vanderbilt, Phys. Rev. B **65**, 035109 (2001).

[37] A. A. Mostofi, J. R. Yates, Y. S. Lee, I. Souza, D. Vanderbilt, and N. Marzari, Comput. Phys. Commun. **178**, 685 (2008).

[38] T. M. Rice and M. Sigrist, J. Phys.: Condens. Matter **7**, L643 (1995).

[39] I. I. Mazin and D. J. Singh, Phys. Rev. Lett. **82**, 4324 (1999).

[40] C. Noce and M. Cuoco, Phys. Rev. B **59**, 2659 (1999).

[41] I. I. Mazin, D. A. Papaconstantopoulos, and D. J. Singh, Phys. Rev. B **61**, 5223 (2000).

[42] E. Pavarini and I. I. Mazin, Phys. Rev. B **74**, 035115 (2006).

[43] M. W. Haverkort, I. S. Elfimov, L. H. Tjeng, G. A. Sawatzky, and A. Damascelli, Phys. Rev. Lett. **101**, 026406 (2008).

[44] E. J. Rozbicki, J. F. Annett, J.-R. Souquet, and A. P. Mackenzie, J. Phys.: Condens. Matter **23**, 094201 (2011).

[45] M. Cuoco, C. Noce, and A. Romano, Phys. Rev. B **57**, 11989 (1998).

[46] J. Spalek, Phys. Rev. B **63**, 104513 (2001).

[47] J. Mravlje, M. Aichhorn, T. Miyake, K. Haule, G. Kotliar, and A. Georges, Phys. Rev. Lett. **106**, 096401 (2011).

[48] V. B. Zabolotnyy *et al.*, New J. Phys. **14**, 063039 (2012).

[49] S. Liu, H. Weng, D. Mou, W. Zhang, Q. Wu, J. He, G. Liu, L. Zhao, H. Liu, X. Jia, Y. Peng, S. He, X. Dong, J. Zhang, Z. Q. Mao, C. Chen, Z. Xu, X. Dai, Z. Fang, and X. J. Zhou, Phys. Rev. B **86**, 165112 (2012).

[50] C. N. Veenstra, Z.-H. Zhu, B. Ludbrook, M. Capsoni, G. Levy, A. Nicolaou, J. A. Rosen, R. Comin, S. Kittaka, Y. Maeno, I. S. Elfimov, and A. Damascelli, Phys. Rev. Lett. **110**, 097004 (2013).

[51] T. Oguchi, Phys. Rev. B **51**, 1385 (1995).

[52] D. J. Singh, Phys. Rev. B **52**, 1358 (1995).

[53] A. Liebsch and A. Lichtenstein, Phys. Rev. Lett. **84**, 1591 (2000).

[54] O. Chmaissem, J. D. Jorgensen, H. Shaked, S. Ikeda, and Y. Maeno, Phys. Rev. B **57**, 5067 (1998).

[55] X. Gonze, B. Amadon, P. M. Anglade, J.-M. Beuken, F. Bottin, P. Boulanger, F. Bruneval, D. Caliste, R. Caracas, M. Côté, T. Deutsch, L. Genovese, P. Ghosez, M. Giantomassi, S. Goedecker, D. R. Hamann, P. Hermet, F. Jollet, G. Jomard, S. Leroux, M. Mancini, S. Mazevet, M. J. T. Oliveira, G. Onida, Y. Pouillon, T. Rangel, G.-M. Rignanese, D. Sangalli, R. Shaltaf, M. Torrent, M. J. Verstraete, G. Zerah, and J. W. Zwanziger, Comput. Phys. Commun. **180**, 2582 (2009).

[56] R. Matzdorf, Z. Fang Ismail, Jiandi Zhang, T. Kimura, Y. Tokura, K. Terakura, and E. W. Plummer, Science **289**, 746 (2000).
[57] A. Tamai, M. P. Allan, J. F. Mercure, W. Meevasana, R. Dunkel, D. H. Lu, R. S. Perry, A. P. Mackenzie, D. J. Singh, Z. X. Shen, and F. Baumberger, Phys. Rev. Lett. **101**, 026407 (2008).
[58] A. V. Puchkov, Z.-X. Shen, and G. Cao, Phys. Rev. B **58**, 6671 (1998).
[59] D. J. Singh and I. I. Mazin, Phys. Rev. B **63**, 165101 (2001).
[60] Q. Huang, J. W. Lynn, R. W. Erwin, J. Jarupatrakorn, and R. J. Cava, Phys. Rev. B **58**, 8515 (1998).
[61] C. Piefke and F. Lechermann, Phys. Status Solidi B **248**, 2269 (2011).
[62] Y. Yanase, J. Phys. Soc. Jpn. **82**, 044711 (2013).
[63] C. Autieri, M. Cuoco, and C. Noce, Phys. Rev. B **85**, 075126 (2012).